Biosensors and Bioelectronics 177 (2021) 112983

Contents lists available at ScienceDirect

Biosensors and Bioelectronics

journal homepage: http://www.elsevier.com/locate/bios

Cryopreservation of a cell-based biosensor chip modified with elastic polymer fibers enabling ready-to-use on-site applications

Dua Özsoylu [a,b], Tuğba Isık [d,e], Mustafa M. Demir [d], Michael J. Schöning [a,c,*], Torsten Wagner [a,c,**]

[a] Institute of Nano- and Biotechnologies (INB), Aachen University of Applied Sciences, Campus Jülich, 52428, Jülich, Germany
[b] Medical Biology and Genetics, Graduate School of Health Sciences, Dokuz Eylül University, Balcova, 35340, Izmir, Turkey
[c] Institute of Biological Information Processing (IBI-3), Research Centre Jülich GmbH, 52425, Jülich, Germany
[d] Department of Materials Science and Engineering, Izmir Institute of Technology, 35430, Izmir, Turkey
[e] School of Chemistry, University of Bristol, Bristol, UK

ARTICLE INFO

Keywords:
On-sensor cryopreservation
Cryo-chip
Ready-to-use
Light-addressable potentiometric sensor
Chemical imaging
Extracellular acidification

ABSTRACT

An efficient preservation of a cell-based biosensor chip to achieve a ready-to-use on-site system is still very challenging as the chip contains a living component such as adherent mammalian cells. Herein, we propose a strategy called on-sensor cryopreservation (OSC), which enables the adherent cells to be preserved by freezing (−80 °C) on a biosensor surface, such as the light-addressable potentiometric sensor (LAPS). Adherent cells on rigid surfaces are prone to cryo-injury; thus, the surface was modified to enhance the cell recovery for OSC. It relies on i) the integration of elastic electrospun fibers composed of polyethylene vinyl acetate (PEVA), which has a high thermal expansion coefficient and low glass-transition temperature, and ii) the treatment with O_2 plasma. The modified sensor is integrated into a microfluidic chip system not only to decrease the thermal mass, which is critical for fast thawing, but also to provide a precisely controlled micro-environment. This novel cryo-chip system is effective for keeping cells viable during OSC. As a proof-of-concept for the applicability of a ready-to-use format, the extracellular acidification of cancer cells (CHO-K1) was evaluated by differential LAPS measurements after thawing. Results show, for the first time, that the OSC strategy using the cryo-chip allows label-free and quantitative measurements directly after thawing, which eliminates additional post-thaw culturing steps. The freezing of the chips containing cells at the manufacturing stage and sending them via a cold-chain transport could open up a new possibility for a ready-to-use on-site system.

1. Introduction

Cell-based biosensors play an outstanding role in all areas of major biomedical research including drug discovery, cancer research, immunology, stem cell research, and regenerative medicine (Gupta et al., 2019). These biosensors, which use cells as a living model system, allow performing experiments and reducing the need for animal testing. Basically, the cells to be investigated are cultured on sensor chips and their cellular response to selected experimental stimuli (e.g., biomolecules, drugs, chemicals) is measured quantitatively and non-invasively (Wasilewski et al., 2020; Pan et al., 2019; Gupta et al., 2019). Monitoring of cellular metabolism is undoubtedly one of the most important issues in the field of cell-based biosensors.

Cellular metabolism is the set of biochemical reactions called metabolic pathways. Glycolysis and cellular respiration are important metabolic pathways for the production of energy (catabolism) in cells. These pathways use major nutrients such as glucose and oxygen to produce energy for the cell while the by-products of the reactions such as lactate, CO_2 and H^+ ions are released to the extracellular environment (Mookerjee et al., 2015). These by-products cause extracellular acidification, which can be used as a sign for abnormal regulations of these energy-related pathways that are mostly associated with extensive diseases such as obesity (Agrawal and Prakash, 2014), schizophrenia (Sullivan et al., 2019), as well as cancer, neurodegeneration, and diabetes (DeBerardinis and Thompson, 2012). Therefore, monitoring of the extracellular acidification using cell-based biosensors has a tremendous

* Corresponding author. Institute of Nano- and Biotechnologies (INB), Aachen University of Applied Sciences, Campus Jülich, 52428, Jülich, Germany.
** Corresponding author. Institute of Nano- and Biotechnologies (INB), Aachen University of Applied Sciences, Campus Jülich, 52428, Jülich, Germany.
E-mail addresses: schoening@fh-aachen.de (M.J. Schöning), torsten.wagner@fh-aachen.de (T. Wagner).

https://doi.org/10.1016/j.bios.2021.112983
Received 21 July 2020; Received in revised form 30 December 2020; Accepted 5 January 2021
Available online 8 January 2021

value in understanding the biological fundamentals of these common diseases.

Only a few cell-based biosensors have been developed for label-free, non-invasive and quantitative sensing of extracellular acidification, including optical methods using the Seahorse XF analyzer (Agilent Technologies Inc., USA) to monitor oxygen consumption (OCR) and extracellular acidification rate (ECAR) (Wu et al., 2007), semiconductor-based methods using the Bionas Discovery 2500 (Bionas GmbH) for real-time monitoring of ECAR (Thedinga et al., 2007), and field-effect-type methods using an ion-sensitive field-effect transistor (ISFET), which seem to be more suitable for long-term measurements of extracellular acidification (Lee et al., 2009). Another field-effect-based biosensor, the light-addressable potentiometric sensor (LAPS), exhibits remarkable features over existing biosensor solutions through its uncomplicated spatial resolution ability. A desired sensing point on the sensor surface can be addressed by light illumination to monitor the extracellular acidification through its pH-sensitive transducer layer. In addition, by using this unique feature, a defined area can be scanned by a modulated light beam to obtain a two-dimensional chemical image of extracellular pH (pH_e) and extracellular acidification (EA). More details regarding the working principle of LAPS can be found elsewhere (Wagner et al., 2016; Schöning et al., 2005b; Yoshinobu et al., 2001; Poghossian et al., 2001; Parak et al., 1997, 2000).

Biosensor systems mentioned above consist of two main components: the sensor itself and cells. The cells, which are frozen in a vial, are delivered to the end-users by cold-chain transportation. To obtain an operational cell-based biosensor system from these two main components, several preparation steps of cell culture such as thawing, centrifugation, counting, seeding, incubation for attachment, adhesion, spread and cell-cell connection and optimization of the cells should be carried out. These preparation steps usually take days (Cheng et al., 2015; Jiang et al., 2018; Park et al., 2019) and operations are limited only to those facilities with established cell culture infrastructure and experienced staff for cell culturing. In addition, potential variations in these preparation steps from facility-to-facility or operator-to-operator might lead to run-to-run variabilities, resulting in less comparable results (Zhao and Fu, 2017). Instead of delivering the biosensors and cells to the end-user separately, preparing the entire system at the manufacturing stage (e.g., mass production) and transporting it to the end-users in a standard and ready-to-use concept could be a solution to overcome the above described drawbacks. However, in this case, the cells inside the sensor system are very demanding for certain vital parameters such as oxygen, nutrients, pH and temperature, which must be carefully kept in balance during transportation to the end-user (Banerjee et al., 2013). Providing these parameters is often not practicable during conventional transportation. Therefore, the storability of cells in a healthy state within a portable system is critical for their practical applicability and commercialization (Ye et al., 2019; Gupta et al., 2019). Thus, there is an urgent need for preserving the whole optimized culture in biosensor applications to enable a ready-to-use on-site system.

Cryopreservation, the process of freezing and preserving cells at subzero temperatures, and thawing them on-demand at a later time, could help to fill the gap in the applications mentioned above. Even though several studies have revealed the benefits of the cell cryopreservation while they adhere to a substrate surface (Beier et al., 2011; Davidson et al., 2015; Kondo et al., 2016; Bissoyi et al., 2016; Bailey et al., 2019), no work using a biosensor as a substrate surface has been reported yet. Therefore, the present work aims to enable an efficient cryopreservation of the whole optimized culture on a biosensor chip. However, for such a cryopreservation the used tools should be designed according to the needs, whose aim has to ensure high cell recovery. For example, the system should provide a rapid removal of the cryoprotectant after thawing and a high surface-area-to-volume ratio enabling rapid warming, which is critical for cell recovery. From this perspective, microfluidic chips are an emerging tool being used in the cryopreservation, and they could also provide a flexibility on microscale integration of other tools (e.g., sensors) for an all-in-one concept (Zhao and Fu, 2017). While some other benefits of such cryo-chips on cell cryopreservation have recently been reported (Bissoyi et al., 2016; Kondo et al., 2016), the surface/biomaterial aspects should be carefully considered because adherent cells are more prone to cryo-injury, which is most likely due to a mismatch in the coefficient of linear thermal expansion between the frozen cell membrane and the rigid substrate in contact. The mismatch could result in a damage of cell membrane, cell detachment, and cell breakage (Beier et al., 2011; Rutt et al., 2019; Batnyam et al., 2017). This effect could also occur in cell-based biosensors that have usually a rigid sensor surface, such as LAPS. Therefore, innovative methods and tools must be implemented to overcome these challenges and to ensure a high cell recovery.

In this study, to enable an efficient preservation of a cell-based biosensor chip in a ready-to-use on-site format, the rigid culture surface of the LAPS is modified with elastic electrospun fibers composed of polyethylene vinyl acetate (PEVA), which has a high thermal expansion coefficient and low glass-transition temperature. The modified sensor is then integrated into a microfluidic chip system for precise control of the microenvironment inside the channels as well as for reducing the thermal mass around the cells to enable fast thawing, which is vital for cell survival. For the first time, the strategy called on-sensor cryopreservation (OSC) has been utilized using this biosensor system (cryo-chip). The performance of this cryo-chip has been validated not only by testing the viability and recovery of the cells (here, CHO-K1) in response to the cryopreservation but also by monitoring their extracellular acidification. An illustrative schematic of the four-step workflow of the procedure is outlined in Fig. 1a-d. The main hypothesis of this study is that the implementation of PEVA electrospun fibers on the LAPS enables a hybrid (elastic/rigid) sensor surface that ensures a better cell recovery for the introduced OSC. As the cryopreservation should provide better cell recovery, optimizing the sensor surface for the OSC-method is one of the main aims of this work. Hence, this work describes both sensor and OSC. Soon, this cryo-chip system can also be used for rapid comparison of the effects of different cryopreservation conditions on the cell recovery, which is one of the main demands in the field of cryobiology.

2. Material and methods

2.1. Sensor fabrication and electrochemical characterizations

The LAPS is made of an Al/p-Si/SiO_2/Ta_2O_5 structure. To obtain this structure, a p-doped silicon wafer (<100>, specific electrical resistivity: 5–10 Ωcm, thickness: 400 μm) was used to grow a thin (30 nm) insulating layer of SiO_2 by thermal dry oxidation procedure (40 min at 1000 °C, O_2). A tantalum (Ta) layer with a thickness of 30 nm was deposited on top of the SiO_2 layer by electron-beam evaporation (0.5 nm/s, 6×10^{-6} mbar). Thereafter, a pH-sensitive transducer layer (60 nm Ta_2O_5) was grown from this layer by a thermal dry oxidation step (520 °C, 120 min). At the rear side, a 300 nm aluminum (Al) layer was deposited as an ohmic contact by electron-beam evaporation (2 nm/s). The wafer was then diced into single chips with the size of 2×2 cm^2. To create an illumination window (1.5×1.5 cm^2) on the rear side of the chip, the Al layer was partially removed by using 5% hydrofluoric acid.

Electrochemical characterization techniques were carried out after sensor fabrication to study sensor functionality by measuring leakage-current-, impedance- and capacitance-voltage (C/V) curves using an

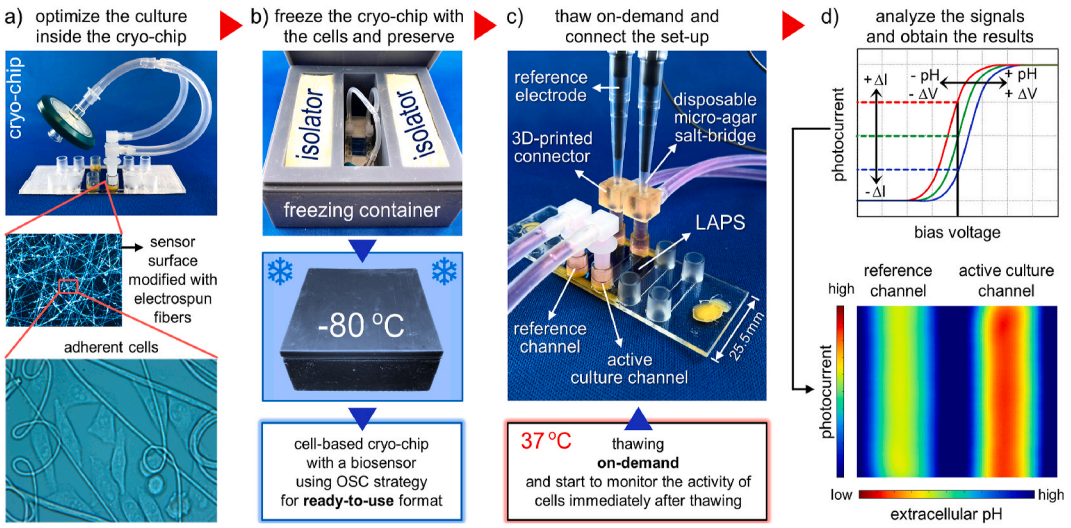

Fig. 1. On-sensor cryopreservation (OSC) offers ready-to-use on-site format for cell-based lab-on-a-chip devices: a) Photo of cryo-chip where a single sensor (LAPS) chip, which was modified with elastic electrospun PEVA fibers, is integrated in the microfluidic system. The system contains two identical and separated microchannels to realize the OSC of adherent cells. b) 3D-printed freezing container designed for cryo-chips ensuring a standardized cooling rate. c) Photo of differential measurement set-up of the chip device. d) Schematic photocurrent vs. voltage (I/V) curves obtained from the set-up and representative differential chemical image to visualize the extracellular acidification inside the channels. The freezing container is available for up to 3 cryo-chips.

electrochemical spectrum analyzer (Zahner-Elektrik GmbH) (Schöning et al., 2005a; Poghossian et al., 2004). For photocurrent-voltage (I/V) measurements, a custom-made scanning LAPS set-up was used as previously described (Wagner et al., 2006; Özsoylu et al., 2019). The sensor characteristics such as pH sensitivity, drift and hysteresis were determined by utilizing Titrisol buffers (Titrisol, Merck, Germany) between pH 5–9.

2.2. Surface modification and characterization

The sensor surface was functionalized with elastic PEVA fibers using the electrospinning technique. PEVA beads (Sigma-Aldrich, vinyl acetate 40 wt%) were dissolved in a mixture of chloroform and *N,N*-Dimethylformamide (3:2, v/v). The resulting polymer concentration was adjusted to 13% (w/v) and the solution was stirred overnight for complete dissolution. The LAPS chips were cleaned consecutively with acetone, isopropanol, ethanol, and deionized (DI) water for 3 min in an ultrasonic bath before coating. Then, the chips were fixed with a double-sided tape on the collector (aluminum foil). The electrospinning setup for the coating of LAPS chips is schematically depicted in Fig. S1 (Supplementary Information). The viscous PEVA solution was transferred into a 5 mL plastic syringe, a stainless-steel needle (18 gauges) was attached, and the needle was connected to a high voltage power supply of 18 kV (Gamma High Voltage Research Ormond Beach, FL, US). The flow rate was adjusted to 1.5 mL/h by using a micro-infusion pump (New Era NE300 Infusion Pump, Farmingdale, NY, USA). The tip-to-collector distance was set to be 10 cm. More details about the optimization of the electrospinning process were given in the supplementary part (See Supplementary Information). A smooth coating was fabricated on the LAPS chips by 60 s electrospinning of PEVA solution at 20–22 °C temperature and 48–50% relative humidity. The morphological characterization of electrospun fibers was carried out by Scanning Electron Microscopy (SEM) (FEI Quanta250 FEG, Oregon, USA) and digital microscope (Keyence, USA). The fiber diameter distributions and average size of fibers were estimated statistically by using the ImageJ software (National Institutes of Health, USA).

2.3. Plasma treatment and characterization

To increase the hydrophilicity of the modified chip surface, O_2 plasma treatment was performed using a low-pressure plasma system (Femto, Diener Plasma Surface Technology). After the samples were placed into the reaction chamber, O_2 gas was injected at a controlled pressure of 0.2 mbar. A radio-frequency generator was operated at 40 kHz while the excitation power, total gas flow rate, controlled pressure, and plasma exposure duration were 30 W, 20 sccm, 0.2 mbar and 30 s, respectively (Özsoylu et al., 2019). To characterize the wettability alteration after the plasma treatment, water contact angle measurements by means of a sessile drop method (static) were performed under controlled temperature (22 °C) and relative humidity (58–60%) using an optical contact angle measuring device (Data Physics Instruments GmbH, Germany). The measurements were carried out by adding 5 µL of DI water drops in a minimum of three randomly selected spots across the sample surfaces. Images of the drops were acquired 10 s after drop impact to calculate the contact angles by using the software module SCA20 (Data Physics Instruments GmbH, Germany). Surface topography, roughness and area of the samples were analyzed by atomic force microscopy (AFM) (BioMat Workstation, JPK Instruments, Germany). At least three samples were analyzed for the characterizations.

2.4. Cryo-chip arrangement

The modified LAPS chip was fixed to the rear side of a bottomless self-adhesive microfluidic slide (sticky-Slide VI 0.4; ibidi GmbH, Germany) to form two identical microchannels on the sensor surface (Fig. 1a). The biocompatible adhesive of this microfluidic slide is precisely aligned to the adhesion areas, thus that the bonding of the chip did not cause any obstruction to the sensor surface or the microfluidic channel itself. In general, the sensor chip is vulnerable to stretches caused by bending. Thus, a biocompatible, two-component epoxy adhesive (EP 655-T, Polytec PT GmbH, Germany) was used to properly seal and encapsulate the edges of the sensor not only to strengthen the adhesion against potential liquid leakage but also to mechanically support it. For sensors treated with plasma, the above-mentioned bonding was performed immediately after the plasma activation. The sensor chip together with the microfluidic channels creates the so-called cryo-chip, which was used to perform the OSC. The width and height of the microchannels are 3.8 mm and 400 µm, respectively. The volume of each microchannel is 30 µL and the volume of each reservoir is 60 µL. A more detailed view of the cryo-chip from different angles to demonstrate

the design concept is shown in Fig. S2 (see Supplementary Information). To ensure the sterility and to prevent complications due to the expansion of the cryoprotectant solution as it freezes, a filter set was prepared by using a 0.22 μm sterile filter and tubes, connected with Y-style tube fitting (Fig. 1a).

2.5. Cell culturing and analysis

Chinese hamster ovary (CHO-K1) cells (DSMZ, Germany) were cultured with the mixture of Ham's Nutrient Mixture F-12/Dulbecco's Modified Eagle Medium (Ham's F-12/DMEM, 1:2 mixture, pH 7.4), supplemented with 5% fetal calf serum (FCS), 100 U/mL penicillin and 100 mg/mL streptomycin (Sigma Aldrich). Cells were incubated inside an incubator providing 37 °C humidified and 5% CO_2-containing atmosphere. To keep the cells healthy, the medium was replaced every 2 days by fresh medium. When the cells became confluent (80–90%), they were passaged in a new culture flask to increase the cell numbers for the next experiments as well as to maintain the cells in the exponential growth.

Once, a sufficient amount of cells was obtained, 4×10^4 cells/cm^2 were seeded inside the channels of the cryo-chip, which were previously sterilized by 70% ethanol for 1 h. As control samples, unmodified LAPS chips and elastic polymer coverslips (uncoated, 180 μm thick, ibidi GmbH, Germany) were used after they were mounted in the same way to the bottomless microfluidic slides (see Section 2.4). The culture medium was replaced with fresh one every 24 h (by pipetting). After the cells were incubated for 48 h, the cell viability was analyzed using a Cell Counting Kit (CCK)-8 assay (Dojindo Laboratories, Kumamoto, Japan). CCK-8 test solution at a 1:10 dilution in the medium was prepared and sterilized by filtering through a filter (0.2 μm pore size). After the channels were washed three times with this solution, the cells were incubated in the incubator with the same solution for 1 h. Negative control samples (without cells) were also prepared and the same procedure was performed. After the incubation, the solution in each channel was thoroughly mixed to ensure homogenous concentration of the formazan dye produced by the cell activity, and it was transferred in a 96-well plate. The absorbance (A) was measured at 450 nm with a reference wavelength of 650 nm on a microplate reader (Spark, Tecan Group Ltd., Switzerland) and it was calculated as follows (see Eq. (1)):

$$A = \left(\text{Absorbance}_{\text{test group}}\right) - \left(\text{Absorbance}_{\text{blank group without cells}}\right) - \left(\text{Absorbance}_{\text{reference at 650 nm}}\right). \quad (1)$$

2.6. On-sensor cryopreservation and thawing

In the next step, after the CKK-8 assay (see Section 2.5) the same cryo-chips with cells were used for cryopreservation. The channels of the cryo-chip were washed twice with a cryoprotectant solution comprised of 90% FCS supplemented with 10% dimethyl sulfoxide (DMSO) and subsequently, the channels were filled with this solution. The filter sets were connected to the inlet and the outlet of the channels. Thereafter, the cryo-chips were placed in a 3D-printed freezing container (Fig. 1b), and then transferred to a −80 °C freezer. The freezing container was designed and printed by a stereolithography (SLA) 3D printer (for details, see Fig. S3 in Supplementary Information). The cryo-chips were kept in the freezer overnight (at least 12 h). The frozen cryo-chip was thawed as rapidly as possible by transferring it directly to the incubator (37 °C). The cryoprotectant solution inside the channels was removed by flushing the channels three times with fresh culture medium (37 °C) as soon as the ice crystals disappeared. The cells were analyzed immediately after thawing and after an incubation for 12 h with the method described in Section 2.5. The cell recovery was calculated as follows (see Eq. (2)):

$$\text{Recovery} = \left(\text{A}_{\text{after thawing}}\right) \;/\; \left(\text{A}_{\text{before freezing}}\right) \times 100\%. \quad (2)$$

All experiments were repeated at least three times. All data presented in this work were shown as the means and standard deviation (SD) unless otherwise indicated. Statistical significance between populations was calculated by using one-way ANOVA followed by Bonferroni post-hoc analysis; a P-value of <0.05 is considered as significant.

2.7. Differential detection of extracellular acidification after OSC

The cryo-chip, composed of the LAPS chip modified with the electrospun PEVA fibers, treated with the O_2 plasma, was used for the following proof-of-concept measurements. One of the two channels of the cryo-chip was identified as a "reference channel" (without cells), while the other was identified as an "active culture channel" (with cells). This enables differential measurements between the channels with and without cells. The cell culturing, cryopreservation and thawing were performed as described in Sections 2.5 and 2.6. All application steps except cell seeding were performed in the same way for both channels. After thawing, the cryoprotectant solution within the channels was immediately replaced with a modified measurement medium, which consists of the Ham's F-12 cell culture medium supplemented with 25 mM D-glucose, 5% FCS, 100 U/mL penicillin and 100 mg/mL streptomycin. No sodium bicarbonate or 4-(2-hydroxyethyl)-1-piperazineethanesulfonic acid (HEPES) were used as the medium should not be highly buffered during the measurements. A self-made micro-agar salt-bridge was developed inside the tip of disposable micropipette tips (200 μL)(Fig. 1c); and it was sterilized using an autoclave to maintain the sterility inside the cryo-chip during the measurements. The details about the preparation steps of this salt-bridge are summarized in Fig. S4 (Supplementary Information). The 3D-printed connectors, tubes and 10 mL glass syringe containing the measurement medium were assembled under aseptic conditions in a laminar flow cabinet. A controlled pump system (neMESYS290N, Cetoni) was applied to supply the medium to the cells inside the channels. A 3D-printed adapter to create an ohmic rear side connection of the LAPS was attached to the cryo-chip (Fig. S2, Supplementary Information); then, it was placed in a self-developed scanning LAPS measurement set-up containing two identical reference electrodes (DriRef-2SH, World Precision Instruments Ltd) and a heated plate for temperature control (ibidi GmbH, Germany), set to 37 °C. Differential scanning LAPS measurements were carried out to monitor the extracellular acidification of the cells. Fig. 1d illustrates how a chemical image is obtained: For both channels, the chemical images were recorded at a constant bias voltage of 0.4 V obtained from the inflection points of the previously recorded I/V curves. More details of the measurement mode of LAPS can be found elsewhere (Miyamoto et al., 2013; Özsoylu et al., 2020). The channels of the cryo-chip were scanned step-wise with a width of 200 μm. In this way, an image composed of 19 × 46 measurement spots was obtained for each channel, which is exemplarily shown in Fig. 1d, bottom part. To correctly evaluate the photocurrent change for each measurement point, internal normalization by subtracting the possible drift effect observed in the reference channel was performed as follows (see Eq. (3)):

$$\text{I}_\text{n} = \left[\left(\text{I}_{\text{AC after thawing}}\right) - \left(\text{I}_{\text{AC initial}}\right)\right] - \left[\left(\text{I}_{\text{RC after thawing}}\right) - \left(\text{I}_{\text{RC initial}}\right)\right]. \quad (3)$$

where I_n is the normalized photocurrent, I_{AC} is the photocurrent in the active culture channel, and I_{RC} is the photocurrent in the reference channel.

3. Results and discussion

3.1. Surface characteristics

Various characterization techniques, such as scanning electron microscopy (SEM), atomic force microscopy (AFM), digital microscopy and contact angle measurements, were performed to understand the characteristics of the PEVA fibers and various surfaces. The average diameter

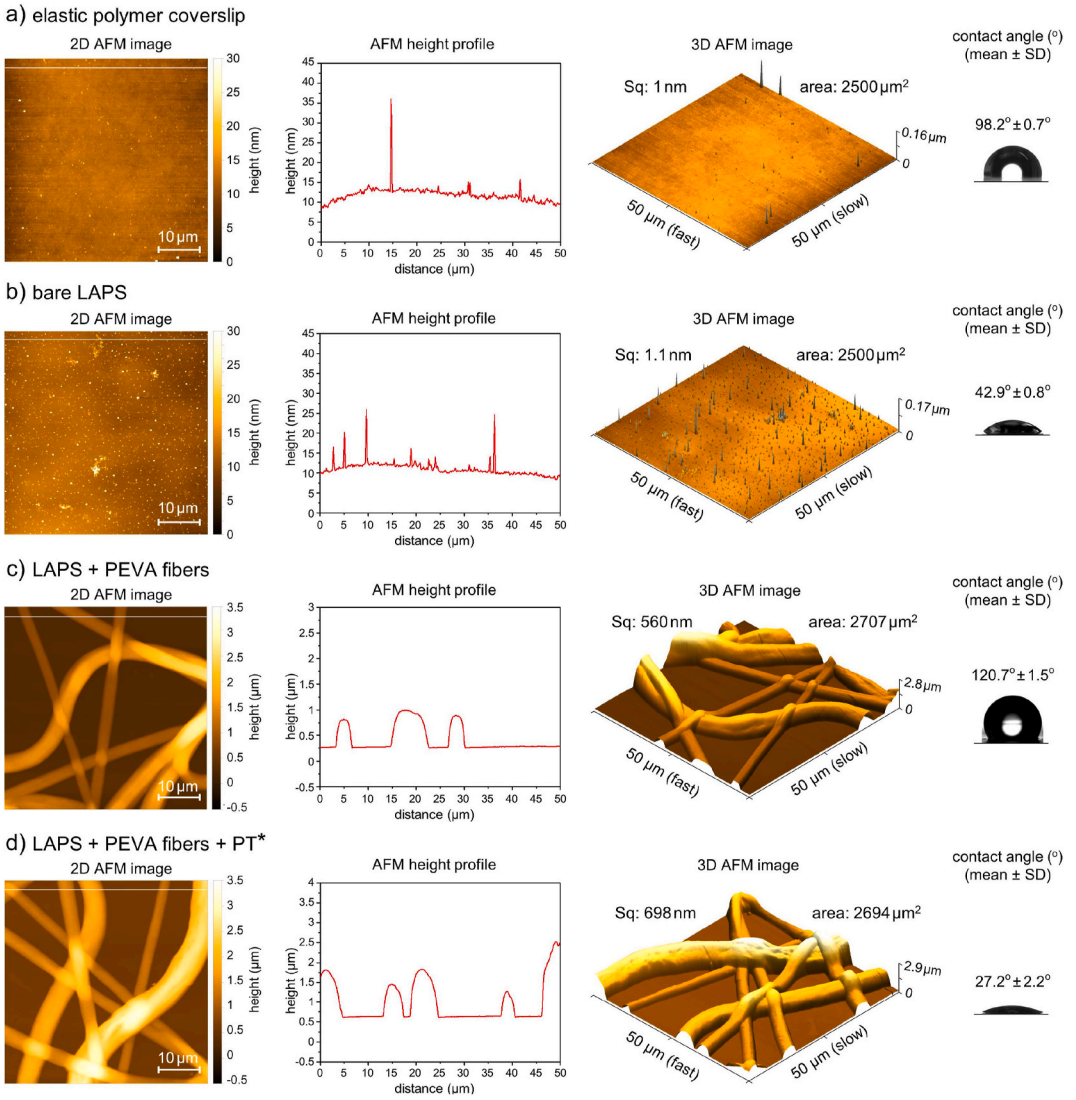

Fig. 2. Surface characteristics such as surface topography and wettability for various surfaces, a) elastic polymer coverslip, b) bare LAPS, c) LAPS modified with PEVA fibers and d) LAPS modified with PEVA fibers and then treated with O_2 plasma. The representative images and a profile graph for each surface are shown under different AFM analysis (2D height image, corresponding height profile and 3D height image) to indicate the surface topography. The representative photos of water droplets for each surface, which were obtained by sessile drop contact angle measurements of deionized (DI) water, indicate the wettability of the surfaces. The mean values of their contact angles, which were obtained from the measurement of the multiple samples, are also presented above each column. Notes: *PT indicates O_2 plasma treatment for 30 s. The AFM height profile for each surface is obtained from the area depicted in the corresponding 2D AFM image, along the trace indicated in white. Sq: Root mean square (RMS) roughness; area: Surface area.

of PEVA electrospun fibers was 3.3 ± 0.5 µm. Fig. 2 depicts other surface characteristics such as surface topography and wettability. The representative 2D AFM height image, line profile, 3D AFM image and contact angle value are shown for each sample, elastic polymer coverslip (Fig. 2a), bare LAPS (Fig. 2b), LAPS modified with PEVA fibers (Fig. 2c) and LAPS with PEVA fibers and O_2 plasma treatment (Fig. 2d). The surface roughness of the bare LAPS (1.14 nm ± 0.61 nm) was slightly higher than that of the coverslip (1.03 nm ± 0.47 nm); however, the difference was statistically not significant ($p = 0.63$). The modification of the LAPS surface with the PEVA fibers notably increased the surface roughness from 1.03 nm ± 0.47 nm to 597.29 nm ± 220.24 nm. After plasma treatment, the roughness stayed almost the same as 597.83 nm ± 123.09 nm ($p = 0.99$). Similarly, the surface area for per projected area (2500 µm^2) increased to 2683.8 µm^2 ± 106.4 µm^2 after modification with PEVA fibers. After plasma treatment, the surface area did not change significantly as 2705.7 µm^2 ± 71.6 µm^2 ($p = 0.74$). Moreover, the hydrophilic LAPS surface (Fig. 2b) was turned into a hydrophobic state (high contact angle values) by the attachment of the fibers (Fig. 2c). The low wettability might be attributed to the increased roughness of the surface (Chen et al., 2018), which comes from the incorporation of PEVA fibers (Fig. 2c). As wettability is one of the most important factors to enhance cell-substrate interaction and cells mostly tend to prefer hydrophilic surfaces (Chen et al., 2018), O_2 plasma treatment was performed to obtain again a hydrophilic surface (low contact angle) (Fig. 2d). The treatment did not influence the integrity of the fibers (Fig. S5, Supplementary Information). Almost all fibers were in contact with the LAPS surface as the fibers coalesced one with the other in junctions and also formed a melded and flattened morphology on the sensor surface (Fig. S6, Supplementary Information).

3.2. Cell responses to on-sensor cryopreservation (OSC)

The morphology and viability of the CHO-K1 cells were analyzed just before and after performing the OSC, as these parameters are fundamentally important to provide evidence about their general health and response to the process of freezing and thawing on different surfaces.

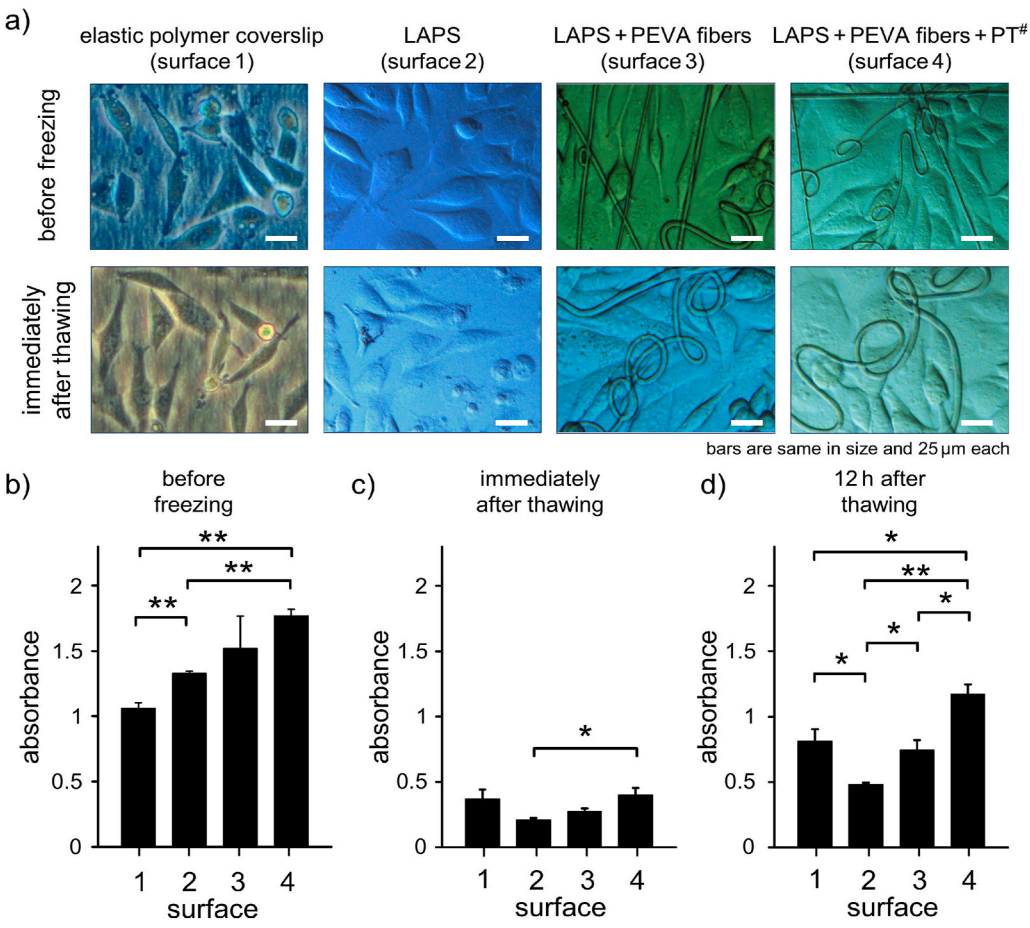

Fig. 3. Cell responses to the OSC (−80 °C, overnight) using the cryo-chip. a) Representative microscopic images of CHO-K1 cells on various surfaces to depict the cell morphology before freezing and immediately after thawing (#PT indicates O_2 plasma treatment for 30 s). Absorbance values from CCK-8 analysis to show the cell viability on the surfaces as elastic polymer coverslip (surface 1), LAPS (surface 2), LAPS modified with PEVA fibers (surface 3), and LAPS modified with PEVA fibers and treated with O_2 plasma (surface 4) b) before freezing, c) immediately after thawing, and d) 12 h after thawing; (*$p < 0.01$, **$p < 0.001$). Note: Absorbance was calculated by subtracting the absorbance of the blank (no cells) from the absorbance of the test sample to eliminate the background absorbance (for details, see Section 2.5).

Before freezing, the cells grown on the LAPS surface, which was modified with PEVA fibers, represented their typical morphological characteristics being well-spread, polygonal in shape and elongated as epithelial cells (Porter et al., 1973) (Fig. 3a, "surface 3"). The same results were obtained when the modified surface was treated with O_2 plasma ("surface 4"). In contrast, the cells grown on the surface of the polymer coverslip ("surface 1") or the unmodified LAPS ("surface 2") mostly showed a spindle-like or more rounded-like morphology and the culture could not reach full confluence on these surfaces. These results were in good agreement with the absorbance values before freezing (Fig. 3b), indicating the cell viability analyzed with the cell counting kit-8 (CCK-8) assay. The lowest absorbance values, indicating a relatively low viability, were found on the hydrophobic polymer coverslip ("surface 1"). The cell viability was observed to be high on the LAPS surface modified with PEVA fibers ("surface 3"), although the wettability of this surface has been quite low in Fig. 2c. The high surface area of the electrospun fibers can enhance the interaction between the scaffolds and adsorbed species (e.g., cells, proteins) so that fibrous surfaces are prone to have more adsorption capacity (Leong et al., 2009; Isık et al., 2016; Isık and Demir, 2018). The highest absorbance values, which indicate a relatively high viability, were observed for the LAPS surface modified with PEVA fibers and then treated with O_2 plasma ("surface 4") that is correlated with the enhanced wettable property of the surface (Fig. 2d). Above all, many other parameters such as chemical composition, stiffness and elasticity of the polymer could cause a synergistic effect for the cell behavior, leading to the improved adsorption on the sensor surface.

Immediately after thawing, most cells cryopreserved on the unmodified LAPS surface showed a cryo-injury phenotype characterized by a disrupted membrane and released cytosol (Fig. 3a, "surface 2"). Partial detachment of the cell monolayer was also observed on this surface (Fig. S7, Supplementary Information). Conversely, the cells cryopreserved on other surfaces displayed the same morphology as they showed before freezing (Fig. 3a). These observations were also validated by analyzing the cell viability. The lowest cell viability was seen on the unmodified LAPS surface (Fig. 3c, "surface 2"). Remarkably, it was noticed that the cell viability was also high on the elastic polymer coverslip (Fig. 3c, "surface 1"), although the lowest viability had been seen in this surface before freezing (Fig. 3b, "surface 1"). Possible explanations for this behavior with regard to the surface elasticity are discussed in detail in the next paragraph. The absolute absorbance values for all surfaces decreased immediately after thawing versus before freezing. This is usually attributed to the thermal shock and mechanical stress for the cells during the freezing and thawing process. Thus, the cells were allowed to recover by an incubation within the cryo-chip for 12 h after thawing (Fig. 3d), which is also important to observe the cell progress such as possible post-thawing cell death (Baust et al., 2009). After the incubation, the highest viability was observed again for the LAPS surface, which was modified with PEVA fibers and then treated with O_2 plasma (Fig. 3d, "surface 4").

Fig. 4 depicts the cell recovery in response to OSC. The highest recovery among the sensor surfaces was seen on the LAPS surface, modified with elastic PEVA fibers and then treated with O_2 plasma ("LAPS + fibers + PT"). The differences between "elastic polymer coverslip" and "LAPS + fibers + PT" were not statistically significant ($p = 0.053$). The beneficial effects of elastic polymers on adherent cell cryopreservation were previously discussed in literature (Rutt et al., 2019; Batnyam et al., 2017; Liu and McGrath, 2007). It was hypothesized that the linear thermal expansion coefficient (α_L) of the substrate should match with that of the ice, formed between the substrate and the cell membrane in

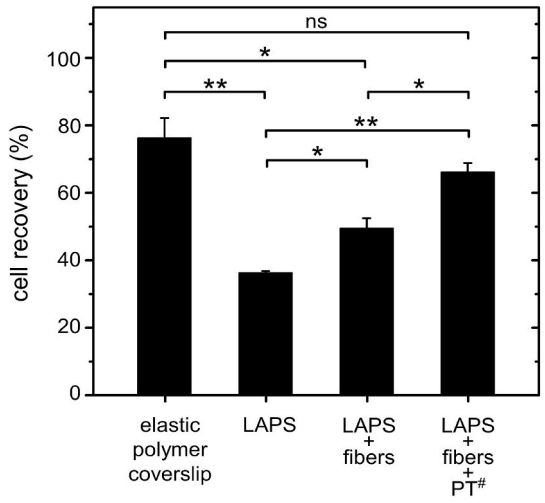

Fig. 4. Comparison of cell recovery obtained by an CCK-8 assay with regard to the OSC (−80 °C, overnight) for various surfaces. The recovery was analyzed according to cell viability just before freezing and 12 h after thawing (for details, see Section 2.6). The error bars represent the standard deviation (SD). #PT indicates O_2 plasma treatment for 30 s *p < 0.01, **p < 0.001, ns: Non-significant (p > 0.05).

contact during the cooling and warming process. Otherwise, different length changes can create gradients of mismatch stress, which are likely relieved through the formation of cracking, blistering, buckling and disintegration (Rutt et al., 2019; Liu and McGrath, 2007). The unmodified LAPS surface consists of Ta_2O_5. The α_L of Ta_2O_5 (3.6×10^{-6}/K) (Tien et al., 2000) is approximately 15 times lower than the α_L of ice (55×10^{-6}/K) (Marchenko, 2018). This difference could be the reason for the low cell recovery (Fig. 4, "LAPS") as well as for the cell detachment and partial monolayer loss observed on the unmodified LAPS samples. Similar observations were previously reported for Chinese hamster fibroblast cells cryopreserved on a rigid glass surface (Rutt et al., 2019). Therefore, the PEVA copolymer with a vinyl acetate (VA) comonomer (weight percent of 40%) was particularly preferred for this study as a higher concentration of vinyl acetate ensures larger α_L values (approx. 550×10^{-6}/K as a polymer film) and elasticity (González-Benito et al., 2015). Although the α_L of PEVA is approximately 10 times higher than the α_L of ice, this mismatch stress could be stored as elastic strain energy in the fibers as the elasticity of the PEVA fibers (Young's modulus of elasticity: approx. 0.0034 GPa) (Wang and Deng, 2019) is highly greater than that of ice (Young's modulus of elasticity: approx. 9 GPa) (Rutt et al., 2019). In addition, the polymer can also keep elasticity until its glass-transition temperature (T_g). In this respect, the PEVA polymer shows superiority with its low T_g (−20 °C) (Wang and Deng, 2019), which is lower than the ice nucleation temperature (usually between −6 °C and −9 °C) in the extracellular compartment, when 10% DMSO was used as a cryoprotective agent (Meneghel et al., 2019). Besides, as it was reported previously (Parizek et al., 2009), the plasma treatment on surfaces can increase the density of focal adhesion points of cells, which could decrease the harmful ice formation between the cell membrane and the substrate in contact (Bissoyi et al., 2016). This might explain the high cell recovery on the samples treated with O_2 plasma after OSC (Fig. 4, "LAPS + fibers + PT"). Moreover, the cells grown and cryopreserved on the elastic polymer coverslip as a reference sample displayed a high cell recovery, although the cell viability had been found to be lower than on other surfaces (Fig. 3b, "surface 1"). This also supports the above-mentioned findings and the hypothesis that the usage of the elastic polymers has beneficial effect on adherent cell cryopreservation (Rutt et al., 2019; Batnyam et al., 2017; Liu and McGrath, 2007).

It is also important to note that the size and shape of the growing ice crystals during freezing and thawing are associated with cell recovery (Biggs et al., 2017). The alterations in surface wettability and topography modulate these characteristics of ice crystals (Li and Guo, 2018); therefore, the increased wettability and roughness (Fig. 2) after modifications of the sensor surface could be associated with the high cell recovery observed in this study. Besides, ice recrystallization (growth in ice crystals, especially during thawing) is another contributor to cryo-injury (Biggs et al., 2017). It should be further explored whether the PEVA exhibits an ice recrystallization inhibition (IRI) activity, which was recently shown in polymers such as poly(vinyl alcohol) (PVA) (Biggs et al., 2019).

3.3. Proof-of-concept measurements

The proposed cryopreservation method (OSC) provides only a benefit if the underlying sensor survives the cryopreservation steps and performs within normal parameter. Only then, a cryo-chip can be used for on-site applications. Thus, the performance of the cryo-chip using the OSC strategy for adherent mammalian cells (CHO-K1) as a model system was validated by differential LAPS measurements after thawing. Fig. 5 depicts three chemical images to visualize the extracellular acidification of the cells after OSC (−80 °C) using the cryo-chip. Fig. 5a shows the chemical image with the photocurrent scale before cell culturing as initial (point zero) measurement performed with the measurement medium (pH 7.4) without cells. As expected, both channels show rather similar photocurrent signals. Thereafter, CHO-K1 cells were cultured only within the active culture channel, and the OSC was performed overnight at −80 °C. Immediately after thawing, both channels were filled with fresh measurement medium (pH 7.4), and connected to the measurement set-up. The chemical image (Fig. 5b) shows that in contrast to the reference channel, the photocurrent values slightly increase in the active culture channel, which indicates not only extracellular acidification but also cell recovery after OSC. Furthermore, the increase of the photocurrent values within the active culture channel was even more visible 6 h after thawing (Fig. 5c). To show these alterations in detail, the average photocurrent values of each channel are given as bar diagrams before cell culturing (Fig. 5d), immediately after thawing (Fig. 5e) and 6 h after thawing (Fig. 5f). Compared to the initial (zero point) photocurrent values of each channel, the average photocurrent change in the active culture channel was 7.2 nA ± 1.1 nA immediately after thawing and 36.6 nA ± 4.7 nA, 6 h after thawing. Instead, the average photocurrent change in the reference channel was −1.8 nA ± 5.7 nA immediately after thawing and −6 nA ± 4.7 nA, 6 h after thawing (Fig. 5g). As there are no cells within the reference channel, the photocurrent changes in this channel indicate a negative sensor signal drift. Despite the fact that these values were rather small, it helps to describe the drift behavior of the overall LAPS chip, which also influences the results of active culture channel. Therefore, this drift behavior should be used to correct the contribution of the extracellular acidification in the active culture channel. For this, differential chemical imaging was implemented by performing a data normalization. This relies on i) subtracting the photocurrent values of each channel (Fig. 5b or Fig. 5c) from their initial (zero point) values (Fig. 5a) and ii) deducting the corresponding drift value seen in the reference channel (Fig. 5g) from the subtracted photocurrent values (for details about the calculation formula, see Section 2.7). In this way, the differential chemical images of the extracellular acidification are shown in Fig. 6.

The optical image of the channels of the cryo-chip after the OSC is displayed in Fig. 6a. This optical image corresponds to the differential chemical images of pH_e with the photocurrent scale immediately after thawing (Fig. 6b) and 6 h after thawing (Fig. 6c). The average increase in the normalized photocurrent in the active culture channel was 9.1 nA ± 1.1 nA immediately after thawing (Fig. 6b) and 42.6 nA ± 4.7 nA, 6 h after thawing (Fig. 6c), which corresponds to a pH shift (acidification) at the LAPS surface of $\Delta pH \approx 0.35$ and $\Delta pH \approx 1.64$, respectively, when considering a pH sensitivity of 26 nA/pH of the LAPS chip. The above-mentioned pH shifts indicate that the average pH value within the

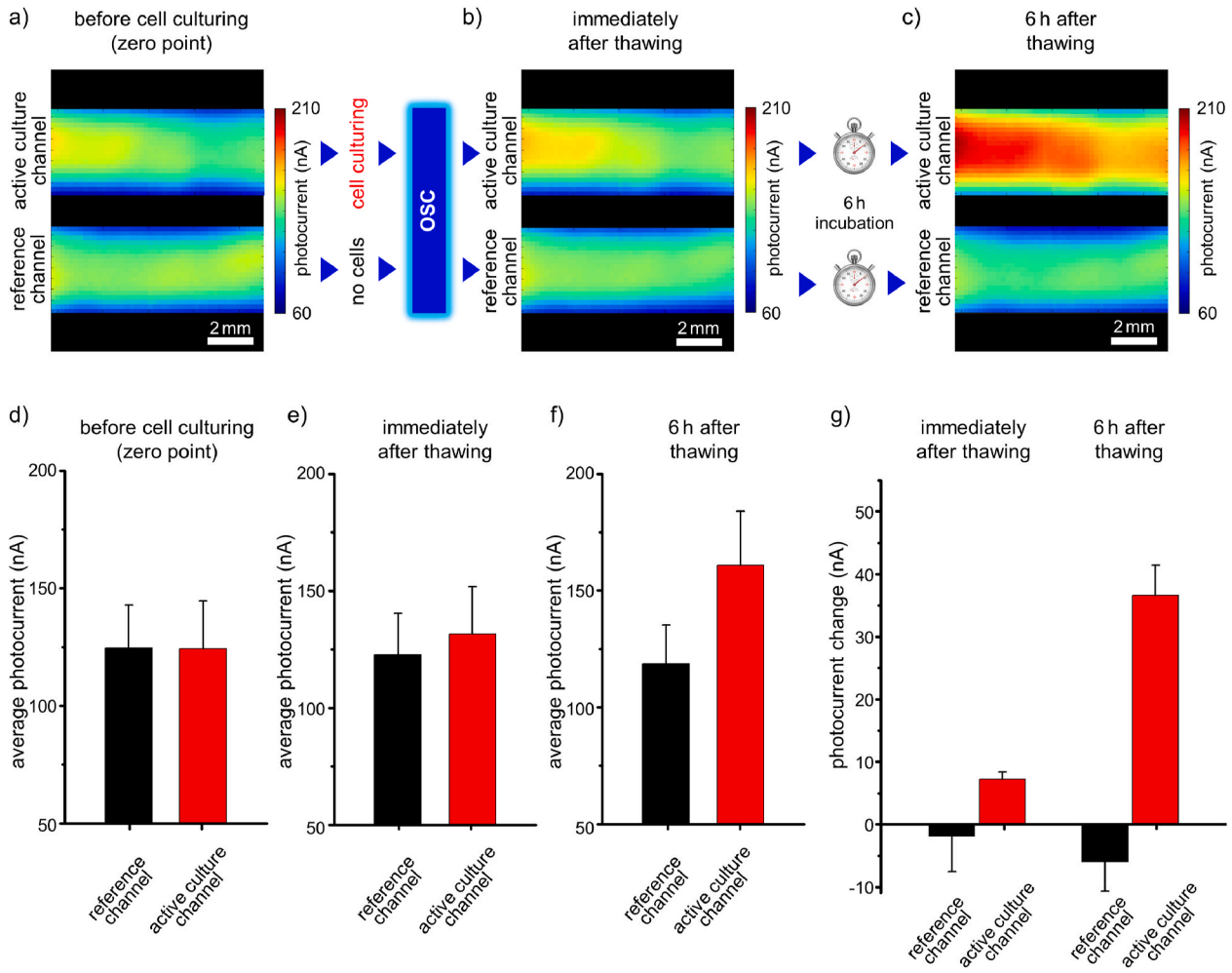

Fig. 5. Post-thawing photocurrent alterations after the OSC of CHO-K1 cells using the two-channel cryo-chip. The chemical images for each channel represent the photocurrent distributions measured a) before cell culturing (zero point), b) immediately after thawing, and c) 6 h after thawing. Comparison of the average photocurrents between the reference channel and the active culture channel corresponding to the chemical images d) before cell culturing (zero point), e) immediately after thawing, and f) 6 h after thawing. g) Photocurrent changes for each individual channel immediately after thawing, and 6 h after thawing. The cryo-chip, modified by electrospun PEVA fibers and treated with O_2 plasma, was used for the cryopreservation (−80 °C, overnight) of the cells in an adherent state. The same measurement medium (pH 7.4) was applied for all measurements. The increase in photocurrent indicates an extracellular acidification.

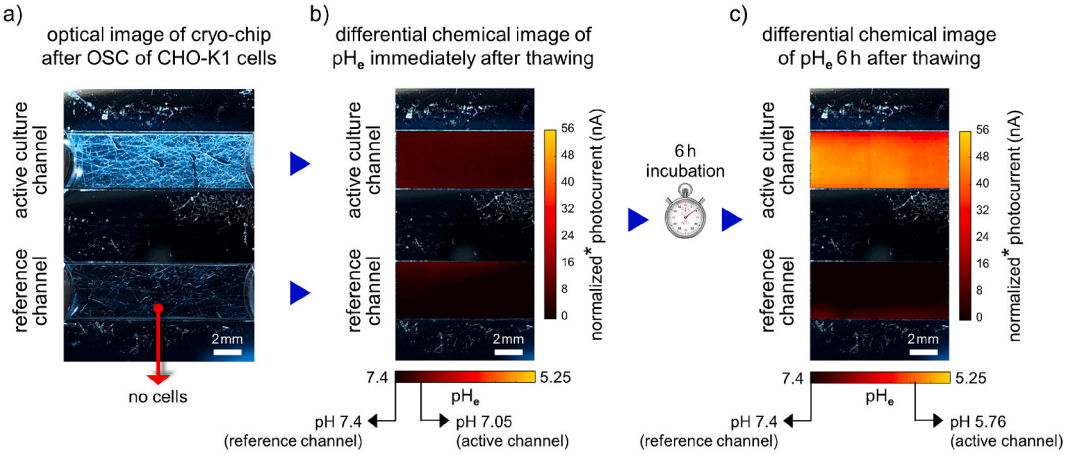

Fig. 6. Differential chemical images of extracellular acidification after the OSC of CHO-K1 cells using the two-channel cryo-chip. a) Optical image of the channels of the cryo-chip after the OSC. Differential chemical images of pH$_e$ b) immediately after thawing, and c) 6 h after thawing. *The normalization was performed by subtracting the photocurrent values of each chemical image from their initial (zero point) values and further subtracting the drift values seen in the corresponding reference channel (for details, see Section 2.7 and Section 3.3). Extracellular pH (pH$_e$) was calculated from the photocurrent difference and the pH sensitivity (26 nA/pH) of the LAPS chip. The increase in photocurrent indicates the extracellular acidification.

active culture channel changed from pH 7.4 to ca. pH 7.05 immediately after thawing and from pH 7.4 to ca. pH 5.76, 6 h after thawing. This extracellular acidification, indicating post-thaw cell viability, also confirms the previous results observed using the CCK-8 assay (Fig. 3c and Fig. 3d, "surface 4"). In terms of the analysis speed, it is worth to note that the utilized CCK-8 assay needs 1–4 h incubation time for the first analysis after thawing. Although some label-based approaches, like lactate dehydrogenase (LDH)- or adenosine triphosphate (ATP)-based assays allow measurement after 10 min incubation, they mostly have some drawbacks such as time-intensive application steps, being an endpoint analysis where the cells are sacrificed by a lysis buffer for analysis, and are potentially interfering with the cellular systems under study (Vetten et al., 2013). The presented cryo-chip system exhibits remarkable superiority through its short preparation time of usually some minutes required for the first analysis. Although the cells could not reach fully metabolic equilibrium in this relatively short time upon thawing, having initial results in a single cryo-chip can still pave the way for rapid comparison of the effects of different cryoprotectant types, concentrations and exposure times on the cell recovery, which is one of the main research topics in cryobiology studies (Katkov et al., 2011; Davidson et al., 2015; Zhao and Fu, 2017; Bailey et al., 2019; Stubbs et al., 2020). In addition, measurements after thawing (around 6–12 h in this study) can reflect the metabolic status of cells for metabolic equilibrium, whereas the incubation can simply be done in cryo-chip and its measurement unit, as an miniaturized incubator is already integrated into it. To the best of our knowledge, this is also the first report to show that analysis of adherent cell activity (herein, extracellular acidification) can be measured immediately after thawing in a label-free, quantitative, and non-invasive manner.

Moreover, the results show that cryopreservation of cells on a biosensor surface and signal analysis after thawing without the need for additional cell culturing steps, e.g., centrifugation, seeding, and immobilization of cells, are possible. Large scale and standardized production of such preserved cryo-chips and cold-chain transportation of them to the end-user could support their practical applicability, that is being in a ready-to-use format even in facilities, which do not have established cell culture infrastructure and skilled staff for cell culturing. This also ameliorates the commercialization potential of cell-based biosensors, which is one of the main challenges in this field (Ye et al., 2019). With recent breakthroughs in biosensors and their integration with organ-on-a-chip (OoC) systems, the need for plug-and-play platforms is increasing in this field day by day (Ashammakhi et al., 2020). Therefore, the presented biosensor chip using OSC strategy could become a key element for these systems to achieve ready-to-use on-site as well as all-in-one solutions.

4. Conclusions and future work

The cryo-chip system introduced in this study using a hybrid (rigid/elastic) structure is effective, compared to an unmodified LAPS surface, for keeping cells viable during on-sensor cryopreservation. A proof-of-concept experiment was performed for the application of the cryo-chip system after OSC with CHO-K1 cells. It was confirmed by chemical images and detection of the extracellular acidification that the cells cryopreserved on the modified sensor surface survived and that the underlying sensor operates within normal parameter, unaltered by the cryopreservation steps. These findings showed, for the first time, that a cryopreservation of adherent cells on a sensor is possible. The introduced cryo-chip system can open up a new possibility for "ready-to-use on-site" applications. Being able to prepare the entire system at the manufacturing stage and to send it via a cold-chain transport further eliminates potential run-to-run and operator-to-operator variability, resulting in more reproducible results.

In future, the new introduced OSC may find applications in the laboratory and the clinical fields. However, the full potential of this concept should also be explored by studying other limited cell types such as stem cells, primary cells, and even organ-like structures such as organoids. Experiments with adherent cells under zero-/micro-gravity are challenging due to the loss of the cell-surface contact and the difficult handling of the cells in space. Here, sending this kind of ready-to-use sensing platform into space could allow to perform extraterrestrial experiments on-site. This could facilitate the real-time monitoring of adherent cells on chip level to study extraterrestrial influences (e.g., cosmic radiation) on cell biology.

CRediT authorship contribution statement

Dua Özsoylu: Writing - original draft, Conceptualization, Investigation, Methodology, Formal analysis, Visualization, Writing - review & editing. **Tuğba Isık:** Investigation. **Mustafa M. Demir:** Formal analysis, Validation. **Michael J. Schöning:** Supervision, Formal analysis, Validation, Writing - review & editing. **Torsten Wagner:** Supervision, Funding acquisition, Validation, Writing - review & editing.

Declaration of competing interest

The authors declare that they have no known competing financial interests or personal relationships that could have appeared to influence the work reported in this paper.

Acknowledgements

Dua Özsoylu (DÖ) would like to acknowledge the PhD research scholarship grant from Scientific and Technological Research Council of Turkey (TÜBITAK) under BIDEB 2214-A. The authors also gratefully thank the Federal Ministry of Education and Research of Germany (Opto-Switch FKZ: 13N12585). This study is a part of PhD thesis study of DÖ (thesis number DEU. HSI. PhD- 2013970198) in Dokuz Eylül University, Institute of Health Sciences, Turkey. Furthermore, the authors would like to thank H. Iken for the LAPS chip processing, D. Rolka for the support in SEM and AFM image analysis, B. Schneider for 3D-printed structures and Th. Schnitzler for the support in cell culturing.

Appendix A. Supplementary data

Supplementary data to this article can be found online at https://doi.org/10.1016/j.bios.2021.112983.

References

Agrawal, A., Prakash, Y., 2014. Obesity, metabolic syndrome, and airway disease. Immunol. Allergy Clin. North Am. 34, 785–796. https://doi.org/10.1016/j.iac.2014.07.004.

Ashammakhi, N., Darabi, M.A., Çelebi–Saltik, B., Tutar, R., Hartel, M.C., Lee, J., Hussein, S.M., Goudie, M.J., Cornelius, M.B., Dokmeci, M.R., Khademhosseini, A., 2020. Microphysiological systems: next generation systems for assessing toxicity and therapeutic effects of nanomaterials. Small Methods 4, 1900589. https://doi.org/10.1002/smtd.201900589.

Bailey, T.L., Stubbs, C., Murray, K., Tomás, R.M.F., Otten, L., Gibson, M.I., 2019. Synthetically scalable poly(ampholyte) which dramatically enhances cellular cryopreservation. Biomacromolecules 20, 3104–3114. https://doi.org/10.1021/acs.biomac.9b00681.

Banerjee, P., Kintzios, S., Prabhakarpandian, B., 2013. Biotoxin detection using cell-based sensors. Toxins (Basel). 5, 2366–2383. https://doi.org/10.3390/toxins5122366.

Batnyam, O., Suye, S.i., Fujita, S., 2017. Direct cryopreservation of adherent cells on an elastic nanofiber sheet featuring a low glass-transition temperature. RSC Adv. 7, 51264–51271. https://doi.org/10.1039/C7RA10604A.

Baust, J.G., Gao, D., Baust, J.M., 2009. Cryopreservation: an emerging paradigm change. Organogenesis 5, 90–96. https://doi.org/10.4161/org.5.3.10021.

Beier, A., Schulz, J., Dörr, D., Katsen-Globa, A., Sachinidis, A., Hescheler, J., Zimmermann, H., 2011. Effective surface-based cryopreservation of human embryonic stem cells by vitrification. Cryobiology 63, 175–185. https://doi.org/10.1016/j.cryobiol.2011.06.003.

Biggs, C.I., Bailey, T.L., Graham, Ben, Stubbs, C., Fayter, A., Gibson, M.I., 2017. Polymer mimics of biomacromolecular antifreezes. Nat. Commun. 8, 1546. https://doi.org/10.1038/s41467-017-01421-7.

Biggs, C.I., Stubbs, C., Graham, B., Fayter, A.E.R., Hasan, M., Gibson, M.I., 2019. Mimicking the ice recrystallization activity of biological antifreezes. when is a new polymer "active"? Macromol. Biosci. 19, 1900082. https://doi.org/10.1002/mabi.201900082.

Bissoyi, A., Bit, A., Singh, B.K., Singh, A.K., Patra, P.K., 2016. Enhanced cryopreservation of MSCs in microfluidic bioreactor by regulated shear flow. Sci. Rep. 6, 35416. https://doi.org/10.1038/srep35416.

Chen, L., Yan, C., Zheng, Z., 2018. Functional polymer surfaces for controlling cell behaviors. Mater. Today 21, 38–59. https://doi.org/10.1016/j.mattod.2017.07.002.

Cheng, M.S., Lau, S.H., Chan, K.P., Toh, C.S., Chow, V.T., 2015. Impedimetric cell-based biosensor for real-time monitoring of cytopathic effects induced by dengue viruses. Biosens. Bioelectron. 70, 74–80. https://doi.org/10.1016/j.bios.2015.03.018.

Davidson, A.F., Glasscock, C., McClanahan, D.R., Benson, J.D., Higgins, A.Z., 2015. Toxicity minimized cryoprotectant addition and removal procedures for adherent endothelial cells. PloS One 10, e0142828. https://doi.org/10.1371/journal.pone.0142828.

DeBerardinis, R.J., Thompson, C.B., 2012. Cellular metabolism and disease: what do metabolic outliers teach us? Cell 148, 1132–1144. https://doi.org/10.1016/j.cell.2012.02.032.

González-Benito, J., Castillo, E., Cruz-Caldito, J.F., 2015. Determination of the linear coefficient of thermal expansion in polymer films at the nanoscale: influence of the composition of EVA copolymers and the molecular weight of PMMA. Phys. Chem. Chem. Phys. 17, 18495–18500. https://doi.org/10.1039/C5CP02384J.

Gupta, N., Renugopalakrishnan, V., Liepmann, D., Paulmurugan, R., Malhotra, B.D., 2019. Cell-based biosensors: recent trends, challenges and future perspectives. Biosens. Bioelectron. 141, 111435. https://doi.org/10.1016/j.bios.2019.111435.

Isık, T., Demir, M.M., 2018. Medical waste treatment via waste electrospinning of PS. Fibers Polym. 19, 767–774. https://doi.org/10.1007/s12221-018-1037-0.

Isık, T., Horzum, N., Yıldız, Ü.H., Liedberg, B., Demir, M.M., 2016. Utilization of electrospun polystyrene membranes as a preliminary step for rapid diagnosis. Macromol. Mater. Eng. 301, 827–835. https://doi.org/10.1002/mame.201600127.

Jiang, D., Liu, Y., Jiang, H., Rao, S., Fang, W., Wu, M., Yuan, L., Fang, W., 2018. A novel screen-printed mast cell-based electrochemical sensor for detecting spoilage bacterial quorum signaling molecules (N-acyl-homoserine-lactones) in freshwater fish. Biosens. Bioelectron. 102, 396–402. https://doi.org/10.1016/j.bios.2017.11.040.

Katkov, I.I., Kan, N.G., Cimadamore, F., Nelson, B., Snyder, E.Y., Terskikh, A.V., 2011. DMSO-free programmed cryopreservation of fully dissociated and adherent human induced pluripotent stem cells. Stem Cell. Int. 2011, 1–8. https://doi.org/10.4061/2011/981606.

Kondo, E., Wada, K.I., Hosokawa, K., Maeda, M., 2016. Cryopreservation of adhered mammalian cells on a microfluidic device: toward ready-to-use cell-based experimental platforms. Biotechnol. Bioeng. 113, 237–240. https://doi.org/10.1002/bit.25704.

Lee, C.S., Kim, S., Kim, M., 2009. Ion-sensitive field-effect transistor for biological sensing. Sensors 9, 7111–7131. https://doi.org/10.3390/s90907111.

Leong, M.F., Chian, K.S., Mhaisalkar, P.S., Ong, W.F., Ratner, B.D., 2009. Effect of electrospun poly(D,L-lactide) fibrous scaffold with nanoporous surface on attachment of porcine esophageal epithelial cells and protein adsorption. J. Biomed. Mater. Res. Part A 89A, 1040–1048. https://doi.org/10.1002/jbm.a.32061.

Li, Q., Guo, Z., 2018. Fundamentals of icing and common strategies for designing biomimetic anti-icing surfaces. J. Mater. Chem. 6, 13549–13581. https://doi.org/10.1039/C8TA03259A.

Liu, B., McGrath, J., 2007. Freezing osteoblast cells attached to hydroxyapatite discs and glass coverslips: mechanisms of damage. Sci. China Ser. E Technol. Sci. 50, 248–256. https://doi.org/10.1007/s11431-007-0021-5.

Marchenko, A., 2018. Thermo-mechanical loads of confined sea ice on structures. Philos. Trans. R. Soc. A Math. Phys. Eng. Sci. 376, 20170341. https://doi.org/10.1098/rsta.2017.0341.

Meneghel, J., Kilbride, P., Morris, J.G., Fonseca, F., 2019. Physical events occurring during the cryopreservation of immortalized human T cells. PloS One 14, e0217304. https://doi.org/10.1371/journal.pone.0217304.

Miyamoto, K.I., Ichimura, H., Wagner, T., Schöning, M.J., Yoshinobu, T., 2013. Chemical imaging of the concentration profile of ion diffusion in a microfluidic channel. Sensor. Actuator. B Chem. 189, 240–245. https://doi.org/10.1016/j.snb.2013.04.057.

Mookerjee, S.A., Goncalves, R.L., Gerencser, A.A., Nicholls, D.G., Brand, M.D., 2015. The contributions of respiration and glycolysis to extracellular acid production. Biochim. Biophys. Acta Bioenerg. 1847, 171–181. https://doi.org/10.1016/j.bbabio.2014.10.005.

Özsoylu, D., Kizildag, S., Schöning, M.J., Wagner, T., 2019. Effect of plasma treatment on the sensor properties of a light–addressable potentiometric sensor (LAPS). Phys. Status Solidi 216, 1900259. https://doi.org/10.1002/pssa.201900259.

Özsoylu, D., Kizildag, S., Schöning, M.J., Wagner, T., 2020. Differential chemical imaging of extracellular acidification within microfluidic channels using a plasma-functionalized light-addressable potentiometric sensor (LAPS). Phys. Med. 10, 100030. https://doi.org/10.1016/j.phmed.2020.100030.

Pan, Y., Hu, N., Wei, X., Gong, L., Zhang, B., Wan, H., Wang, P., 2019. 3D cell-based biosensor for cell viability and drug assessment by 3D electric cell/matrigel-substrate impedance sensing. Biosens. Bioelectron. 130, 344–351. https://doi.org/10.1016/j.bios.2018.09.046.

Parak, W.J., George, M., Domke, J., Radmacher, M., Behrends, J., Denyer, M., Gaub, H., 2000. Can the light-addressable potentiometric sensor (LAPS) detect extracellular potentials of cardiac myocytes? IEEE Trans. Biomed. Eng. 47, 1106–1113. https://doi.org/10.1109/10.855939.

Parak, W.J., Hofmann, U.G., Gaub, H.E., Owicki, J.C., 1997. Lateral resolution of light-addressable potentiometric sensors: an experimental and theoretical investigation. Sensors Actuators A Phys 63, 47–57. https://doi.org/10.1016/S0924-4247(97)80428-1.

Parizek, M., Kasalkova, N., Bacakova, L., Slepicka, P., Lisa, V., Blazkova, M., Svorcik, V., 2009. Improved adhesion, growth and maturation of vascular smooth muscle cells on polyethylene grafted with bioactive molecules and carbon particles. Int. J. Mol. Sci. 10, 4352–4374. https://doi.org/10.3390/ijms10104352.

Park, J.S., Grijalva, S.I., Jung, D., Li, S., Junek, G.V., Chi, T., Cho, H.C., Wang, H., 2019. Intracellular cardiomyocytes potential recording by planar electrode array and fibroblasts co-culturing on multi-modal CMOS chip. Biosens. Bioelectron. 144, 111626. https://doi.org/10.1016/j.bios.2019.111626.

Poghossian, A., Mai, D.T., Mourzina, Y., Schöning, M.J., 2004. Impedance effect of an ion-sensitive membrane: characterisation of an EMIS sensor by impedance spectroscopy, capacitance–voltage and constant–capacitance method. Sensor. Actuator. B Chem. 103, 423–428. https://doi.org/10.1016/j.snb.2004.04.071.

Poghossian, A., Yoshinobu, T., Simonis, A., Ecken, H., Lüth, H., Schöning, M.J., 2001. Penicillin detection by means of field-effect based sensors: EnFET, capacitive EIS sensor or LAPS? Sensor. Actuator. B Chem. 78, 237–242. https://doi.org/10.1016/S0925-4005(01)00819-X.

Porter, K., Prescott, D., Frye, J., 1973. Changes in surface morphology of Chinese hamster ovary cells during the cell cycle. J. Cell Biol. 57, 815–836. https://doi.org/10.1083/jcb.57.3.815.

Rutt, T., Eskandari, N., Zhurova, M., Elliott, J.A., McGann, L.E., Acker, J.P., Nychka, J.A., 2019. Thermal expansion of substrate may affect adhesion of Chinese hamster fibroblasts to surfaces during freezing. Cryobiology 86, 134–139. https://doi.org/10.1016/j.cryobiol.2018.10.006.

Schöning, M.J., Brinkmann, D., Rolka, D., Demuth, C., Poghossian, A., 2005a. CIP (cleaning-in-place) suitable "non-glass" pH sensor based on a Ta_2O_5-gate EIS structure. Sensor. Actuator. B Chem. 111–112, 423–429. https://doi.org/10.1016/j.snb.2005.03.053.

Schöning, M.J., Wagner, T., Wang, C., Otto, R., Yoshinobu, T., 2005b. Development of a handheld 16 channel pen-type LAPS for electrochemical sensing. Sensor. Actuator. B Chem. 108, 808–814. https://doi.org/10.1016/j.snb.2005.01.055.

Stubbs, C., Bailey, T.L., Murray, K., Gibson, M.I., 2020. Polyampholytes as emerging macromolecular cryoprotectants. Biomacromolecules 21, 7–17. https://doi.org/10.1021/acs.biomac.9b01053.

Sullivan, C.R., Mielnik, C.A., Funk, A., O'Donovan, S.M., Bentea, E., Pletnikov, M., Ramsey, A.J., Wen, Z., Rowland, L.M., McCullumsmith, R.E., 2019. Measurement of lactate levels in postmortem brain, iPSCs, and animal models of schizophrenia. Sci. Rep. 9, 5087. https://doi.org/10.1038/s41598-019-41572-9.

Thedinga, E., Kob, A., Holst, H., Keuer, A., Drechsler, S., Niendorf, R., Baumann, W., Freund, I., Lehmann, M., Ehret, R., 2007. Online monitoring of cell metabolism for studying pharmacodynamic effects. Toxicol. Appl. Pharmacol. 220, 33–44. https://doi.org/10.1016/j.taap.2006.12.027.

Tien, C.L., Lee, C.C., Chuang, K.P., Jaing, C.C., 2000. Simultaneous determination of the thermal expansion coefficient and the elastic modulus of Ta_2O_5 thin film using phase shifting interferometry. J. Mod. Optic. 47, 1681–1691. https://doi.org/10.1080/09500340008231417.

Vetten, M.A., Tlotleng, N., Tanner Rascher, D., Skepu, A., Keter, F.K., Boodhia, K., Koekemoer, L.A., Andraos, C., Tshikhudo, R., Gulumian, M., 2013. Label-free in vitro toxicity and uptake assessment of citrate stabilised gold nanoparticles in three cell lines. Part. Fibre Toxicol 10, 50. https://doi.org/10.1186/1743-8977-10-50.

Wagner, T., Rao, C., Kloock, J., Yoshinobu, T., Otto, R., Keusgen, M., Schöning, M.J., 2006. "LAPS card"- a novel chip card-based light-addressable potentiometric sensor (LAPS). Sensor. Actuator. B Chem. 118, 33–40. https://doi.org/10.1016/j.snb.2006.04.019.

Wagner, T., Vornholt, W., Werner, C.F., Yoshinobu, T., Miyamoto, K.I., Keusgen, M., Schöning, M.J., 2016. Light-addressable potentiometric sensor (LAPS) combined with magnetic beads for pharmaceutical screening. Phys. Med. 1, 2–7. https://doi.org/10.1016/j.phmed.2016.03.001.

Wang, K., Deng, Q., 2019. The thermal and mechanical properties of poly(ethylene-co-vinyl acetate) random copolymers (PEVA) and its covalently crosslinked analogues (cPEVA). Polymers 11, 1055. https://doi.org/10.3390/polym11061055.

Wasilewski, T., Kamysz, W., Gębicki, J., 2020. Bioelectronic tongue: current status and perspectives. Biosens. Bioelectron. 150, 111923. https://doi.org/10.1016/j.bios.2019.111923.

Wu, M., Neilson, A., Swift, A.L., Moran, R., Tamagnine, J., Parslow, D., Armistead, S., Lemire, K., Orrell, J., Teich, J., Chomicz, S., Ferrick, D.A., 2007. Multiparameter metabolic analysis reveals a close link between attenuated mitochondrial bioenergetic function and enhanced glycolysis dependency in human tumor cells. Am. J. Physiol. Physiol. 292, C125–C136. https://doi.org/10.1152/ajpcell.00247.2006.

Ye, Y., Guo, H., Sun, X., 2019. Recent progress on cell-based biosensors for analysis of food safety and quality control. Biosens. Bioelectron. 126, 389–404. https://doi.org/10.1016/j.bios.2018.10.039.

Yoshinobu, T., Ecken, H., Poghossian, A., Simonis, A., Iwasaki, H., Lüth, H., Schöning, M.J., 2001. Constant-current-mode LAPS (CLAPS) for the detection of penicillin. Electroanalysis 13, 733–736. https://doi.org/10.1002/1521-4109(200105)13:8/9<733::AID-ELAN733>3.0.CO;2-N.

Zhao, G., Fu, J., 2017. Microfluidics for cryopreservation. Biotechnol. Adv. 35, 323–336. https://doi.org/10.1016/j.biotechadv.2017.01.006.